# Shape memory polymers modeling (a tentacle)

Christian Lexcellent*, Pauline Butaud*, Emmanuel Foltête*, Morvan Ouisse*

*Univ. Bourgogne Franche-Comt, FEMTO-ST Institute, CNRS/UFC/ENSMM/UTBM, Department of Applied Mechanics, 25000 BESANON-FR*

## 1. Introduction

The mechanisms associated to the thermomechanical behavior of shape memory polymers are very different of the martensitic phase transformation exhibited by shape memory alloys (change of crystalline network between the austenitic "mother" phase and the martensitic "produced" phase) [1].

The thermomechanical properties of shape memory polymers, namely stiffness, Young's modulus, Poisson ratio and thermal expansion coefficient are extremely dependent of temperature since the polymer behavior drastically changes between under and above the glass transition temperature $T_g$. This temperature is related to the so-called "molecules' mobility" which is low under $T_g$ and high above. Some authors may speak about "hard domains" and "soft domains" respectively.

Hence, the shape memory polymers (SMP) can be considered as two-phases materials with[2]:

- a rigid phase corresponding to the "glassy state" when $T < T_g$, $T$ being the temperature and $T_g$ the glass or vitrous transition temperature.The cohesion between the molecular chains is assured by the Van Der Waals forces;
- a soft phase corresponding to the "rubbery state" when $T_g < T < T_f$, $T_f$ being the fusion temperature. A part of the links provided by the Van Der Waals forces is broken inducing higher molecules mobility.

The properties of SMP are most of the time frequency- or strain rate-dependent. In permanent harmonic regime or in the Laplace space, the

*christian.lexcellent@femto-st.fr

applied stress may be written as

$$\sigma(t) = \sigma_0 e^{j\omega t}, \tag{1}$$

where $\sigma_0$ is the magnitude of the stress, $\omega$ the frequency and $j^2 = -1$. The corresponding strain is

$$\varepsilon(t) = \varepsilon_0 e^{j(\omega t - \delta)}, \tag{2}$$

which provides the expression of the complex elasticity modulus $E^*$, namely

$$E^* = \frac{\sigma(t)}{\varepsilon(t)} = \frac{\sigma_0}{\varepsilon_0} e^{j\delta}. \tag{3}$$

This complex modulus can be decomposed in real part and imaginary one:

$$E^*(\omega, T) = E^{'}(\omega, T) + jE^{''}(\omega, T) \ , \tag{4}$$

where $E^{'}$ is called the storage modulus and $E^{''}$ the loss modulus. The loss factor $\eta$ is defined as

$$\eta = \tan\delta = \frac{E''}{E'}. \tag{5}$$

A tipycal evolution of these properties is given by Hayashi [3], which provides some results on a shape memory polyurethane (MM-4520) manufactured by SMP Technologies, which is rigid at room temperature ($T_g \simeq 45$ ℃). In this work, the dynamical mechanical analysis (DMA) was conducted on a Perkin-Elmer DMA instrument, in bending mode, using the dual cantilever attachment on bars with length 20 mm , width 12 mm and thickness 3.5 mm. The single-frequency scanning temperature was run by increasing temperature by 2 ℃ /min, at 1 Hz (figure 1).

In time, the analysis is more complicated, since the transient movement is not described by harmonic analysis, and the time history is required to properly describe the behavior of interest. In the following, we review several models of SMP that may be used in time and frequency analyses.

## 2. A first thermomechanical modeling

### *2.1. Description of the model*

A unidimensional thermomechanical constitutive model is proposed by Tobushi et al. [5], in which nonlinear stress terms are considered for both elastic and viscous effects.

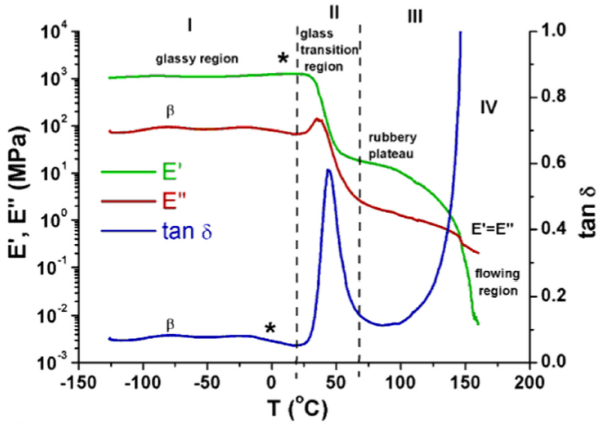


Figure 1: DMA results at 1 Hz for a SMP (MM-4520): variation of the storage modulus $E'$, the loss modulus $E''$ and the loss factor $\tan\delta$ [4].

In these conditions, the authors introduce a non-linear constitutive equation:

$$\dot{\varepsilon} = \frac{\dot{\sigma}}{E} + m\left(\frac{\sigma - \sigma_y}{k}\right)^{m-1}\frac{\dot{\sigma}}{k} + \frac{\sigma}{\mu} + \frac{1}{b}\left(\frac{\sigma}{\sigma_c} - 1\right)^n - \frac{\varepsilon - \varepsilon_s}{\lambda} + \alpha\dot{T}, \tag{6}$$

where $\sigma$, $\varepsilon$, $T$ denote stress, strain and temperature respectively. The dot denotes time derivative. $E$, $\mu$, $\lambda$, and $\alpha$ are the Young's modulus, the viscosity, the retardation time and the coefficient of thermal expansion.

In order to express the non-linear time-independent strain, with respect to linear elastic term $\frac{\dot{\sigma}}{E}$ in equation (6), a non linear term is used, described by a power stress function. The irrecoverable $\varepsilon_s$ is then considered as

$$\varepsilon_s = S(\varepsilon_c + \varepsilon_p). \tag{7}$$

The dependence of coefficients $E$, $k$, $\sigma_y$, $\mu$, $\sigma_c$, $\lambda$, and $S$ are expressed by an exponential function of temperature $T$. These parameters are denoted by $x$ and are written as

$$x(T) = x_g \exp[a(\frac{T_g}{T} - 1)], \tag{8}$$

where $x_g$ is the $x$ value at $T = T_g$. The boundaries of the glass transition region are $T_g \pm T_w$. Each coefficient is constant above $T_g + T_w$ and below $T_g - T_w$.

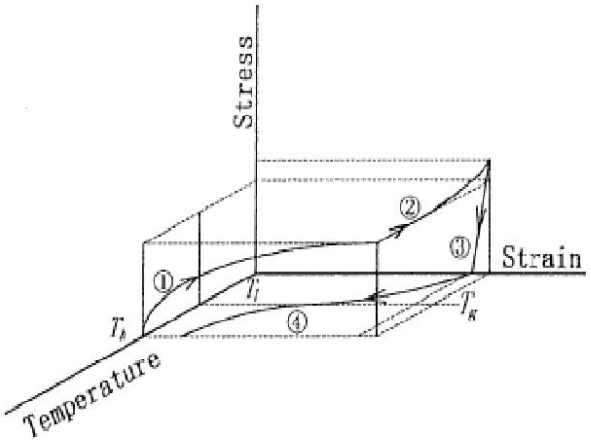


Figure 2: Three dimensional stress-strain-temperature diagram showing the loading path in the thermomechanical test [5].

*2.2. Test description*

In order to validate the model, a three-dimensional stress-strain-temperature diagram in which the thermomechanical tests can be described is used, as shown in figure 2. The successive steps are:

(1) isothermal loading at $T_h = T_g + T_w$ ($T_w = 20\ K$) until $\varepsilon = \varepsilon_m$ (rubbery state),

(2) thermal stress associated to cooling until $T_1 = T_g - T_w$ with $\varepsilon_m$ kept constant,

(3) unloading at $T_1$,

(4) heating until $T_h$.

In the applications presented in the paper, the strain rate is $8.33 \times 10^{-3}\ s^{-1}$, the heating rate is 0.0667 K.s$^{-1}$, the cooling rate is 0.133 K.s$^{-1}$ while $\varepsilon_m =$ 4 %, 10%, and 20%.

*2.3. Stress-strain-temperature relationship*

The values of the parameters ($E_g$, $k_g$, $\sigma_{yg}$, $\mu_g$ , $\sigma_{cg}$, $\lambda_g$ and $S_g$) are determined at $T_g$ [5]. The coefficients above and below $T_g$ are obtained by fitting using equation (8).

As seen in figures 3 and 4, during the loading process (1) up to $\varepsilon_m$ at $T_h$, the stress increases nonlinearly when the strain becomes large. In the cooling process (2), the stress increases.

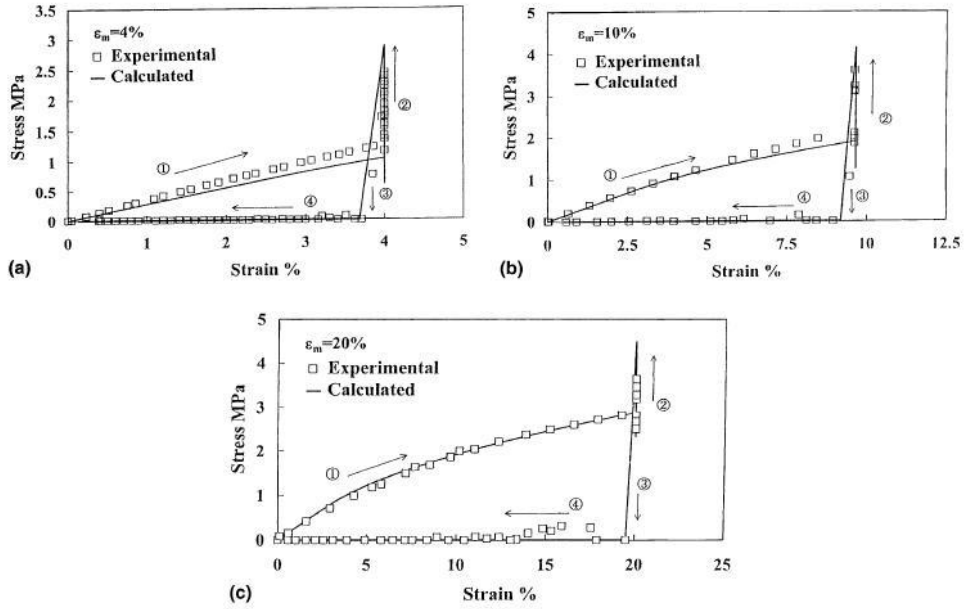


Figure 3: Relationship between stress and strain in the thermomechanical test: (a) $\varepsilon_m = 4\%$, (b) $\varepsilon_m = 10\%$, (c) $\varepsilon_m = 10\%$ [5].

*2.4. Remark concerning modeling*

All the parameters of the model are obtained by curve fitting based on the empirical equation (6). The parameters temperature dependency are given by an exponential form (equation 8). For practical applications, this may be useful but one should mention that this model is not a predictive model.

## 3. A second thermomechanical modeling [6]

The Helmholtz free energy $H_{total}$ of a representative volume of material is obtained from the contribution of the Helmholtz free energy of the rubbery phase $H_r$ and the Helmholtz free energy of the glassy phase $H_g$:

$$H_{total} = f_r(T)H_t + f_g(T)H_g, \tag{9}$$

where the glassy rate $f_g(T) = 1 - f_r(T)$, $f_r$ being the rubbery rate. The authors proposed to introduce "a third phase" called "initial glassy phase" $f_{go}$ such that:

$$H_{total} = f_r(T)H_t + f_{g0}(T)H_{g0} + f_g(T)H_g. \tag{10}$$

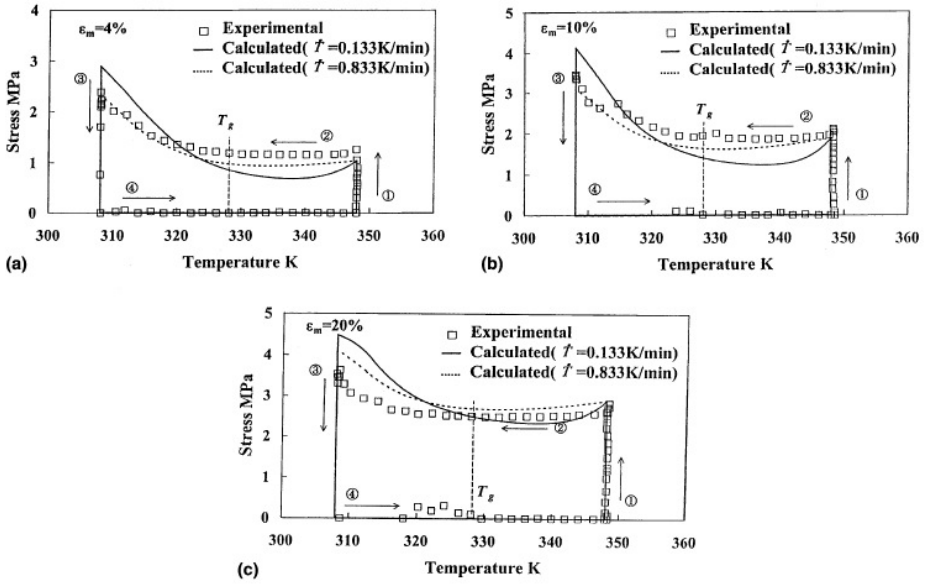


Figure 4: Relationship between stress and temperature in the thermomechanical test: (a) $\varepsilon_m = 4\%$, (b) $\varepsilon_m = 10\%$, (c) $\varepsilon_m = 10\%$ [5].

The total stress is then written as:

$$\boldsymbol{\sigma} = f_r(T)\boldsymbol{\sigma}_{\mathrm{r}} + f_{g0}\boldsymbol{\sigma}_{\mathrm{go}} + f_t\boldsymbol{\sigma}_{\mathbf{t}}. \tag{11}$$

The model has been developed using the Voigt limit and presuming that the volume fraction of each phase is expressed as

$$f_r(T) = \frac{1}{1 + exp(-(T - T_{ref})/A)},\ f_g(T) = 1 - f_r(T). \tag{12}$$

One has to note that $f_r$ or $f_g$ expressions are chosen such that $f_r(T = T_{ref}) = f_g(T = T_{ref}) = \dfrac{1}{2}$. Hence, $T_{ref}$ can be considered as the mean temperature value.

The initial conditions in the model are given by $f_{g0} = f_g(t = 0)$ and $f_t((t = 0)) = 0.0$.

During cooling, one has $f_{g0} = f_g(t = 0)$ and $f_t((t = t_2)) = f_t((t = t_1)) + \Delta f_g$ where $t_2 > t_1$.

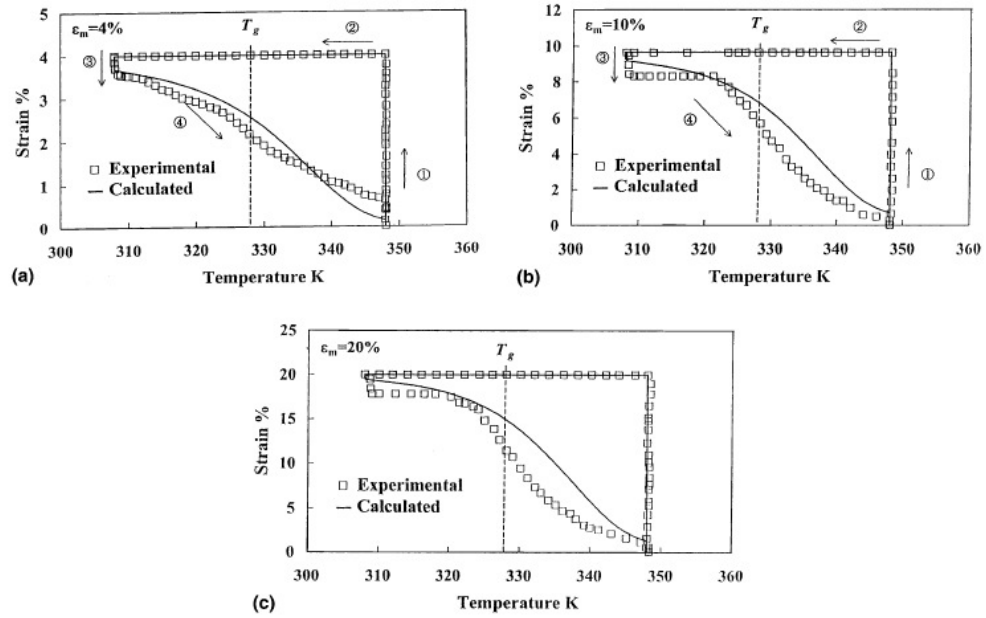


Figure 5: Relationship between strain and temperature in the thermomechanical test: (a) $\varepsilon_m = 4\%$, (b) $\varepsilon_m = 10\%$, (c) $\varepsilon_m = 10\%$ [5].

During reheating, $\Delta f_g$ of glassy phase transforms into rubbery phase (RP). Here both IGP and FGP transform in RP in a similar way. Therefore

$$\Delta f_{g0} = \frac{f_{g0}}{f_{go} + f_t} \Delta f_g \; \Delta f_t = \frac{f_t}{f_{go} + f_t} \Delta f_g, \tag{13}$$

where $\Delta f_{g0}$ is the volume fraction from the IGP and $\Delta f_t$ is the volume fraction from the FGP. Finally one has:

$$f_{g0}(t = t_4) = f_{g0}(t = t_3) - \Delta f_{g0}, \; f_t(t = t_4) = f_t(t = t_3) - \Delta f_t, \tag{14}$$

where $t_4 > t_3$.

### *3.1. Deformations and stresses*

#### *3.1.1. Rubbery phase*

As indicated above, the material response at $T \geq T_g$ shows rubber like hyperelastic behavior. For an isotropic homogeneous elastomer, the Langevin

chain-based Arruda-Boyce eight-chain model [7] captures the hyperelastic behavior of the material up to large stretches. Qi et al. [6] defined the Cauchy stress tensor as:

$$\boldsymbol{\sigma}_{\mathbf{r}} = \frac{\mu_r}{3J_r}\frac{\sqrt{N_r}}{\lambda_{ch}}L^{-1}[\frac{\lambda_{ch}}{\sqrt{N_r}}]\mathbf{B}_{\mathbf{r}}^{'} + k_r(J_r - 1 - 3\alpha_1(T - T_0))\mathbf{1}.\ \lambda_{ch} = \sqrt{tr\mathbf{B}_{\mathbf{r}}/3}, \tag{15}$$

where $k_r$ is the elastic bulk modulus, $\mu_r$ the initial bulk modulus, $N_r$ the number of "rigid links" between the two crosslink sites, $\sqrt{N_r}$ the limit stretch, $\alpha_1$ the thermal expansion coefficient (at $T \geq T_g$), $L^{-1}(x)$ an inverse Langevin function, $\mathbf{1}$ the second order identity tensor. The volumetric strain is obtained from $\overline{\mathbf{F_r}} = (\frac{1}{\mathrm{J_r^{\frac{1}{3}}}})\mathbf{F_r}$ where $\mathbf{F_r}$ is the overall strain gradient, $J_r = det[\mathbf{F_r}]$ ; $\overline{\mathbf{B_r}} = \overline{\mathbf{F_r}}(\overline{\mathbf{F_r}})^T$ and $\overline{\mathbf{B_r}}^{'} = \overline{\mathbf{B_r}} - \frac{1}{3}tr(\overline{\mathbf{B_r}})\mathbf{1}$ is the deviatoric part of $\overline{\mathbf{B_r}}$ ; $\lambda_{ch} = \sqrt{\frac{tr(\overline{\mathbf{B_r}})}{3}}$.

The inverse Langevin function $L^{-1}(x)$ is an integral component for statistically based networks models which describe rubber-like materials. It is defined by

$$L(x) = \coth x - \frac{1}{x}. \tag{16}$$

Among the various approximations of $L^{-1}(x)$, a popular approximation, valid on the whole range $x \in$ ]-1,1[ has been published by A. Cohen [8] as

$$L^{-1}(x) \simeq x\frac{3 - x^2}{1 - x^2}. \tag{17}$$

A more recent contribution from Jedynak [9], which is valid for $x \geq 0$ $x \neq 1$, provides

$$L^{-1}(x) \simeq x\frac{3.0 - 2.6x + 0.7x^2}{(1 - x)(1 + 0.1x)}. \tag{18}$$

*3.1.2. Initial glassy phase*

The deformation of the IGP is represented by the total strain gradient $\mathbf{F}$. Among many models, Qi et al [6] described also the hyperelastic behavior using the method proposed by Arruda-Boyce [7]. The viscoplastic behavior of the polymer is modeled in decomposing the stress response into an equilibrium time-independent behavior and a non-equilibrium time- dependent behavior.

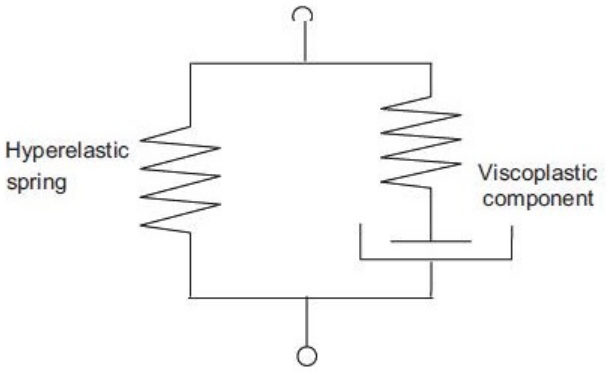


Figure 6: One-dimensional rheologic representation of viscoplastic model of a glassy polymer.

The figure 6 shows a 1D rheological representation of the model. The total stress is:

$$\boldsymbol{\sigma}_{\mathbf{g0}} = \boldsymbol{\sigma}^{\boldsymbol{r}}_{\boldsymbol{g0}} + \boldsymbol{\sigma}^{\boldsymbol{ve}}_{\boldsymbol{g0}}. \tag{19}$$

The hyperelastic spring can be modeled using the Arruda-Boyce eight chain model, but with different parameters i.e.:

$$\boldsymbol{\sigma}^{\mathbf{r}}_{\mathbf{g0}} = \frac{\mu_g}{3J_G}\frac{\sqrt{N_G}}{\lambda_{ch}} L^{-1}[\frac{\lambda_{ch}}{\sqrt{N_G}}]\mathbf{B}'_{\mathbf{g}} + k_g(J_g - 1 - 3\alpha_2(T - T_0))\mathbf{1}. \tag{20}$$

For the viscoplastic deformation, one writes:

$$\mathbf{F}^{\mathrm{e}} = \mathbf{F}\mathbf{F}^{\mathrm{v}^{-1}}. \tag{21}$$

The stress due to viscoplastic deformation can be calculated using $\mathbf{F}^{\mathrm{e}}$ i.e.:

$$\boldsymbol{\sigma}^{\mathbf{ve}}_{\boldsymbol{go}} = \frac{1}{J^e}[\mathbf{L}^{\mathrm{e}} : \mathbf{E}^{\mathrm{e}} - \alpha_{\mathbf{2}}(3\lambda_g + 2G_g)(T - T_0)\mathbf{1}], \tag{22}$$

where $J^e = \det(\mathbf{F}^{\mathrm{e}})$, $\mathbf{E}^{\mathrm{e}} = \ln \mathbf{V}^{\mathrm{e}}$, $\mathbf{V}^{\mathrm{e}} = \mathbf{F}^{\mathrm{e}}\mathbf{R}^{\mathrm{e}}$ and $\mathbf{L}^{\mathrm{e}}$ is the fourth order isotropic elasticity tensor

$$\mathbf{L}^{\mathrm{e}} = 2G_g\underline{\mathbf{1}} + \lambda_g \mathbf{1} \otimes \mathbf{1}, \tag{23}$$

$G_g$ and $\lambda_g$ being the Lam constants and $\underline{\mathbf{1}}$ the fourth-order identity tensor.

The evolution of $\mathbf{F}^{\mathrm{e}}$ is obtained through the decomposition of spatial velocity gradient

$$l = \dot{\mathbf{F}}\mathbf{F}^{-\mathbf{1}} = \dot{\mathbf{F}}^{\mathrm{e}}\mathbf{F}^{e-1} + \mathbf{F}^{\mathrm{e}} l^{v} \mathbf{F}^{e-1}, \tag{24}$$

where $\dot{\mathbf{F}}$ is the material velocity gradient , $l^v = \dot{\mathbf{F}}^{\mathrm{v}}\mathbf{F}^{\mathbf{v}-\mathbf{1}}$is the spatial velocity gradient with:

$$l^v = \dot{\mathbf{F}}^{\mathrm{v}}\mathbf{F}^{\mathbf{v}-\mathbf{1}} = \mathbf{D}^{\mathrm{v}} + \mathbf{W}^{\mathrm{v}}, \tag{25}$$

where $\mathbf{D}^{\mathrm{v}}$ and $\mathbf{W}^{\mathrm{v}}$ are the stretching rate and the spin. For isotropic configuration, the authors used $\mathbf{W}^{\mathrm{v}} = 0$ and choose for the viscoplastic stretch rate

$$\mathbf{D}^{\mathrm{v}} = \frac{\dot{\gamma}^{v}}{\sqrt{2\overline{\tau}}} \overline{\boldsymbol{\sigma}}'_{\mathrm{g0}}, \tag{26}$$

where $\overline{\boldsymbol{\sigma}_{\mathrm{g0}}} = \mathbf{R}^{\mathrm{e}}\boldsymbol{\sigma}_{\mathbf{g0}}\mathbf{R}^{\mathrm{e}}$. Here the prime symbol denotes the deviator $\overline{\tau}$ which is the equivalent shear stress defined as :

$$\overline{\tau} = [\frac{1}{2}\overline{\boldsymbol{\sigma}}'_{\mathrm{g0}} : \overline{\boldsymbol{\sigma}}'_{\mathrm{g0}}]^{\frac{1}{2}}. \tag{27}$$

$\dot{\gamma}^{v}$ denotes the viscoplastic shear strain rate and is described by:

$$\dot{\gamma}^{v} = \dot{\gamma}_0 exp[-\frac{\Delta G}{kT}\{1 - (\frac{\overline{\tau}}{s})\}]. \tag{28}$$

To further consider the softening effects observed in the experiments, the following evolution rule can be used:

$$\dot{s} = h_0(1 - \frac{s}{s_s})\dot{\gamma}^{v} \text{ with } s = s_0 \text{ when } \gamma^{v} = 0, \tag{29}$$

where $s_0$ is the initial value of athermal shear stress and $s_s$ the saturation value. When $s_0 > s_s$, equation (29) represents an evolution rule that characterizes a softening of the material.

*3.1.3. Frozen glassy phase FGP*

During cooling, a new glassy phase will be formed ("frozen" from the rubbery phase RP). The deformation in the RP is also frozen implying that the "newly formed glassy phase" does not inherit the deformation of the RP phase and will behave as an undeformed material. But there is a new strain due to the redistribution of overall strain, the incremental strain gradient for the FGP $\Delta\mathbf{F}_{\mathrm{T}}^{\mathrm{n+1}}$ is:

$$\Delta\mathbf{F}_{\mathrm{T}}^{\mathrm{n+1}} = \{ \begin{array}{c} \mathbf{F}^{\mathrm{n+1}}(\mathbf{F}^{\mathrm{n}}) \; if \; \Delta T \neq 0 \\ \mathbf{1} \text{ if } \Delta \mathrm{T} = 0 \end{array} \}, \tag{30}$$

where $\mathbf{F}^{\mathrm{n}}$ and $\mathbf{F}^{\mathrm{n+1}}$ are the overall strain gradients at the increment $n$ and $n+1$.

The total strain gradient acting on the FGP is written as:

$$\mathbf{F}_{\mathrm{T}}{}^{\mathrm{n+1}} = \Delta\mathbf{F}_{\mathrm{T}}^{\mathrm{n+1}}\mathbf{F}_{\mathrm{T}}^{\mathrm{n}}. \tag{31}$$

The stress in the FGP can be calculated using equations (20)-(31) with $\mathbf{F}_{\mathrm{T}}$ instead of $\mathbf{F}$ in equations (20) and (23).

The definition of the FGP plays a key role in capturing the shape memory effect. The advantage of this definition is that it does not require the introduction of a 3D finite deformation equivalent "stored strain" which was used in 1D small deformation constitutive model of Liu et al. [10].

### *3.2. Results*

The material parameters of the model are identified and listed in table 1.

| Model components | Material parameters | Values |
|---|---|---|
| Thermal expansion coefficients | $\alpha_1(\mathrm{K}^{-1})$ | $2.53 \times 10^{-4}$ |
| | $\alpha_2(\mathrm{K}^{-1})$ | $1.48 \times 10^{-4}$ |
| Volume fraction evolution | $A$ | 7.0 |
| | $T_r$ $(K)$ | 297 |
| Rubbery phase | $\mu_r$ (MPa) | 0.8 |
| | $N_r$ | 17 |
| | $k_r$ (MPa) | $1 \times 10^3$ |
| Glassy phase | $\mu_g$ (MPa) | 0.1 |
| Hyperelastic spring | $N_g$ | 17 |
| | $k_g$ (MPa) | $1 \times 10^3$ |
| Viscoplastic component | $G_g$ (MPa) | $0.47 \times 10^3$ |
| | $\lambda_g$ (MPa) | $1.89 \times 10^3$ |
| | $\Delta G$ $(\times 10^{-19})$ | 0.92 |
| | $\dot{\gamma}_0$ $(s^{-1})$ | 52 |
| | $s_0$ (MPa) | 56 |
| | $s_s$ (MPa) | 28 |
| | $h_0$ (MPa) | 400 |

Table 1: Parameters used in the simulations [6].

#### *3.2.1. Isothermal uniaxial compression simulation*

Figure 7 shows the comparison between experiments and numerical simulations of isothermal uniaxial compressions at different temperatures and strain rates. The effect of temperature and strain rate is shown.

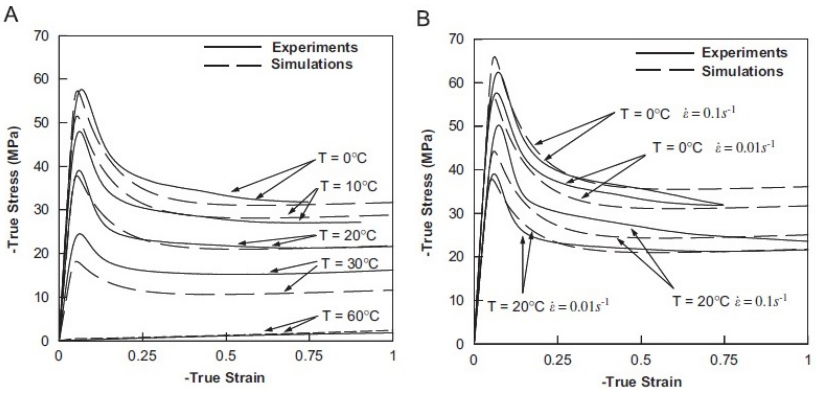


Figure 7: Compression tests [6]

*3.2.2. DMA simulations to determine $T_g$*

A cylindrical sample was subjected to an isothermal uni-axial cyclic loading following a sinusoidal waveform at 1 Hz with a maximum strain of 4%. Figure 8 shows $\tan\delta$ versus temperature. It should be emphasized that the maximum value of the loss factor has been normalized to the maximum value for both numerical and experimental results: the maximum value is not predicted by the model, while the shape of the curve is almost captured.

*3.2.3. Free recovery*

The numerical simulation of the free recovery experiment was conducted to demonstrate the shape memory effect of the model (figure 9).

*3.2.4. Constrained recovery*

In figure 10, the stress was normalized by the maximum compression stress immediately after loading at high temperature. In addition, during heating, a large overshoot in the stress was observed in the experiments but not captured in the model. Heat transfer and stress relaxation which are not included in the model, may explain this fact.

*3.3. Remark concerning modeling*

In the paper of Qi et al[6], the originality comes from that three phases (one rubbery phase and two glassy phases) are considered i.e.: Rubbery Phase (RP) with $T \geq T_g$ ; Frozen Glassy Phase (FGP) which refers to the newly formed glassy phase caused by a decrease in the temperature from

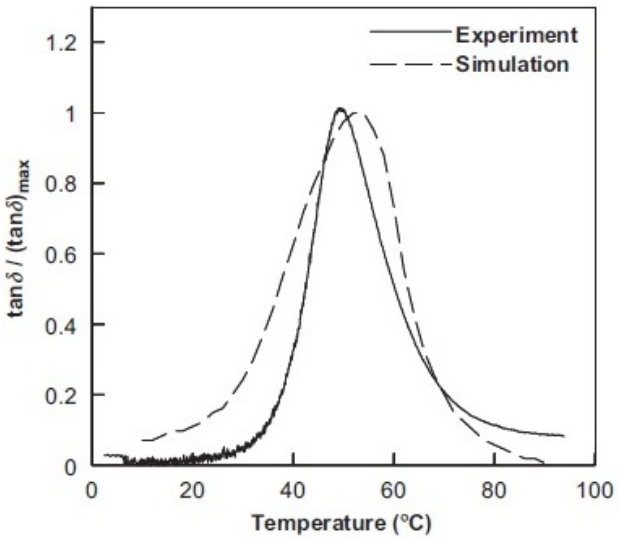


Figure 8: $Tg$determination by cyclic tests [6]

$T \leq T_g$) ; Initial Glassy Phase (IGP) which refers to the glassy phase in the initial configuration of the material.

For RP the Cauchy stress tensor is obtained using an hyperelastic model, namely a Arruda-Boyce eight chain [7]. The IGP stress can be represented by an hyperelastic spring with the same behavior as before combined with a component associated to the viscoplastic deformation. As the initial deformation of FGP is zero, the new strain is due to the redistribution of overall strain. The incremental strain gradient for the FGP $\Delta \mathbf{F_T}^{n+1}$ is defined. Moreover, a guideline for material parameter identification is given. As the authors said, heat transfer and stress relaxation are not included in the model.

## 4. A third thermomechanical modeling [11], [4]

Depending on the studied strain regime, the constitutive models are formulated in large or small deformation frameworks. Pieczyska et al. choose classically the mixture between two phases [11]. The model includes the "hard" glassy phase called $g$ and the "soft" rubbery phase called $r$. There is no more distinction between FGP and IGP but only a glassy phase $g$. The constitutive equations are formulated separately for each phase. A rheological scheme of the 1D model is shown in figure 6.

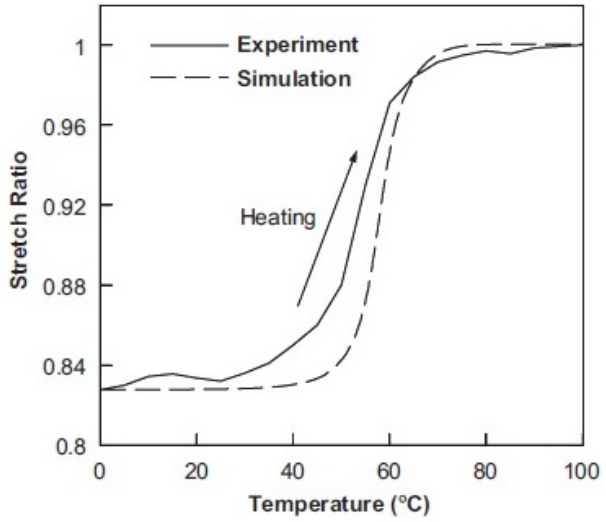


Figure 9: Deformation recovered during reheating in the free recovery case [6].

*4.1. Rubbery phase*

The modeling of this phase is strictly the same as the one used by Qi et al.[6], based on the eight chains model of Arruda-Boyce [7].

*4.2. Glassy phase*

The viscoplastic strain rate tensor $\mathbf{D}_\nu$, is expressed as [11]:

$$\begin{array}{c} \mathbf{D}_\nu = \dot{\gamma}^\nu \mathbf{N}_{\mathrm{g}}^\nu,\ \mathbf{N}_{\mathrm{g}}^\nu = \sqrt{\frac{3}{2}}\boldsymbol{\sigma}_{\mathbf{g}}^{\prime\mathbf{II}}/\tau_{g\nu} \\ \tau_{g\nu} = \sqrt{\frac{3}{2}\boldsymbol{\sigma}_{\mathbf{g}}^{\prime\mathbf{II}} : \boldsymbol{\sigma}_{\mathbf{g}}^{\prime\mathbf{II}}} \end{array}, \tag{32}$$

where $\boldsymbol{\sigma}_{\mathbf{g}}^{\prime\mathbf{II}}$ is the deviator of the Cauchy stress tensor $\boldsymbol{\sigma}_{\mathbf{g}}^{\mathbf{II}}$ and $\dot{\gamma^\nu}$ the equivalent viscoplastic shear rate.

The evolution of the viscoplastic part of $\mathbf{F}_g^{\mathrm{II}}$ is calculated as:

$$\dot{\mathbf{F}_g^\nu} = \dot{\gamma^\nu}(\mathbf{F}_{\mathbf{g}}^{\mathrm{ethII}})^{-1}\mathbf{N}_{\mathrm{g}}^\nu \mathbf{F}_g^{\mathrm{II}}. \tag{33}$$

In a classical way for the equivalent viscoplastic shear rate, a power law is used:

$$\dot{\gamma^\nu} = \dot{\gamma_0}(\frac{\tau_{g\nu}}{\tau_{g\nu}^c})^{m+1}, \tag{34}$$

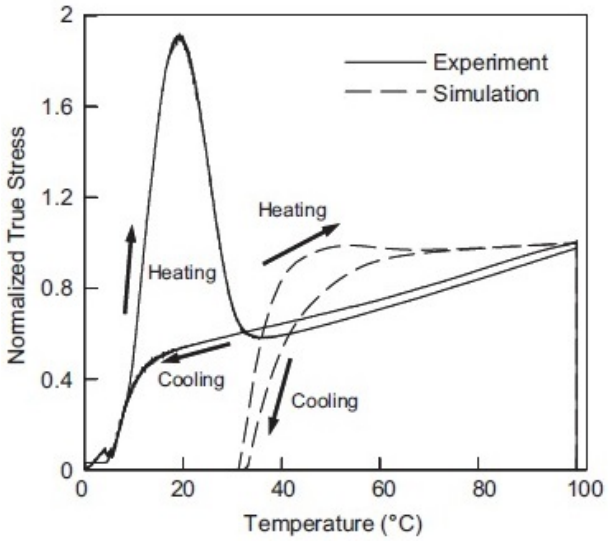


Figure 10: Stress response in the constrained recovery case.[6]

with

$$\tau^c_{g\nu} = \tau_0 exp(-\frac{h_1}{\tau_0}\gamma_\nu) + \tau_{sat}(1 - exp(-\frac{h_0}{\tau_{sat}}\gamma_\nu)). \tag{35}$$

Moreover, some deformation and temperature change measurements with infrared camera are performed during some tensile tests, as shown in figure 11.

*4.3. Overall behavior*

The effective behavior of the shape memory polyurethane is the resultant response of individual phases. Pieczyska et al. [11], [4] choose the Voigt-type averaging scheme, based on a uniform strain hypothesis. The total Cauchy stress tensor $\boldsymbol{\sigma}$ is an average of stresses in the individual phases. Thus, one has:

$$\mathbf{F} = \mathbf{F}_\mathrm{r} = \mathbf{F}_\mathrm{g}\ \boldsymbol{\sigma} = f_r\boldsymbol{\sigma}_\mathbf{r} + f_g\boldsymbol{\sigma}_\mathbf{g}. \tag{36}$$

Qi et al. [6] give the same mixing rule between the "three phases":

$$\boldsymbol{\sigma} = f_r(T)\boldsymbol{\sigma}_\mathrm{r} + f_{g0}\boldsymbol{\sigma}_\mathrm{go} + f_t\boldsymbol{\sigma}_\boldsymbol{t}. \tag{37}$$

This choice corroborates the concluding remarks of Gilormini and Diani [12]. They show that uniform strain hypothesis leads to good predictions whereas a consistent use of the uniform stress hypothesis in order to predict the elastic properties and thermal expansions gives poor results.

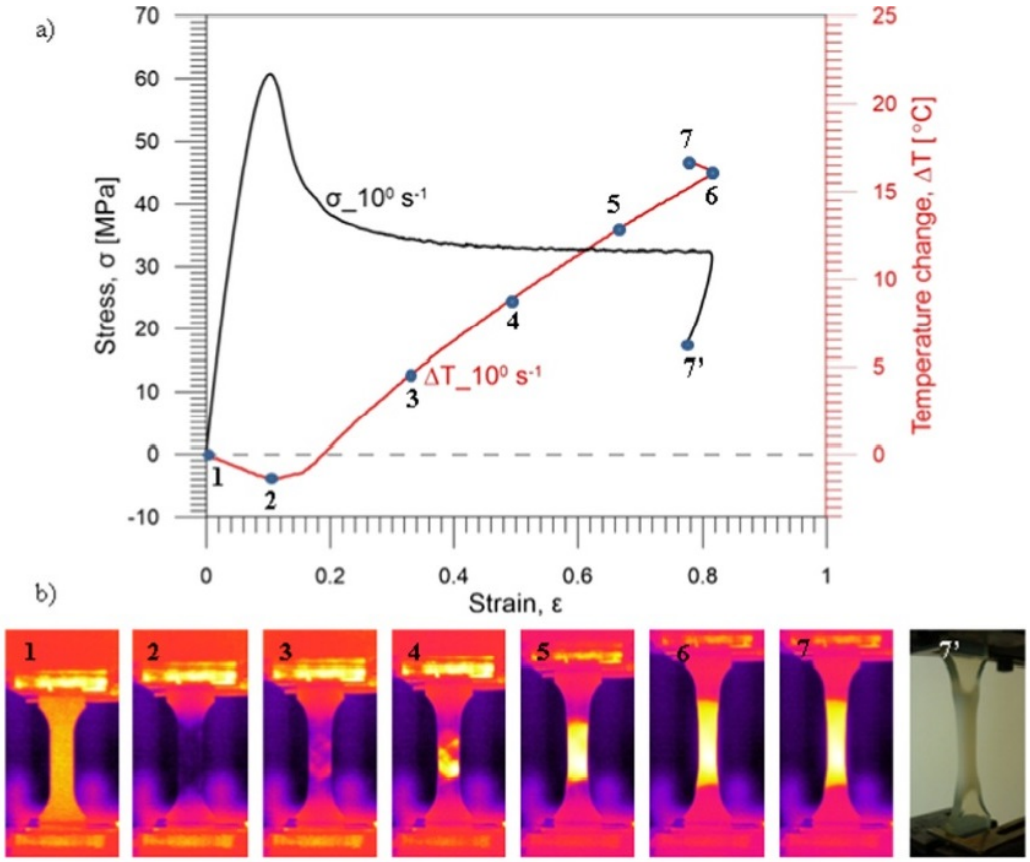


Figure 11: SMP ($T_g = 45$ ℃) tensile test at strain rate 1 $sec^{-1}$ [4]

*4.4. Analysis of the relaxation problem [13]*

Subsequently, the same team tried to solve the problem of modeling the stress response in the constrained recovery case shown in figure 10. They introduced a multi-branch approach for non-equilibrium relaxation processes. A rheological representation of the model is proposed in figure 12.

As usual, hyperelastic material models for rubbers are used for the equilibrium behaviors. For nonequilibrium behaviors in the viscoelastic branches, it is assumed that all branches follow the same viscous flow rules with different relaxation times. As the temperature is varied, the relaxation times in individual branches also vary. The authors [13] assumed that the time-temperature shift for each branch follows the same rule according to the

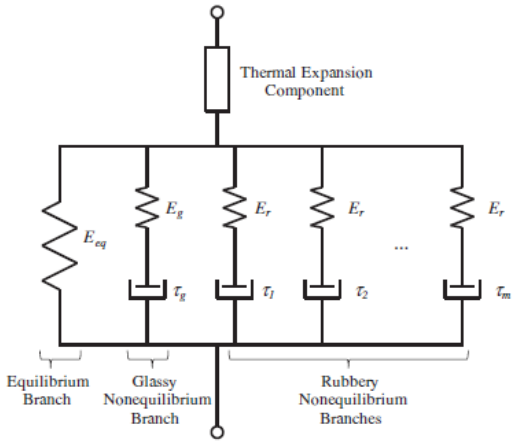


Figure 12: Rheological representation of the proposed model [13].

"thermo-logical simplicity" [14] i.e.

$$\tau_M^i(T) = \tau_0^i a_T(T) \text{ for } i = 1, ..., m+1. \tag{38}$$

At temperatures close to or above $T_g$ The William-Landel-Ferry equation [15] is used:

$$\log a_T = \frac{C_1(T - T_0)}{C_2 + (T - T_0)}. \tag{39}$$

When temperatures are below $T_g$, an Arrhenius- type behavior developed by Di Marzio and Yang [16] is used:

$$\ln a_T = -\frac{AF_c}{k_B}(\frac{1}{T} - \frac{1}{T_g}). \tag{40}$$

For nonequilibrium rubberry branches ($i = 1, ..., m$), each branch is taken to represent a relaxation mode and the Rouse model is chosen.The relaxation times are given by Rubinstein and Colby [14]:

$$\tau_0^i = \frac{\tau_R}{i^2} \text{ for } i = 1, ..., m. \tag{41}$$

Hence, the problem of modeling the constrained recovery cycle (see figure 12).

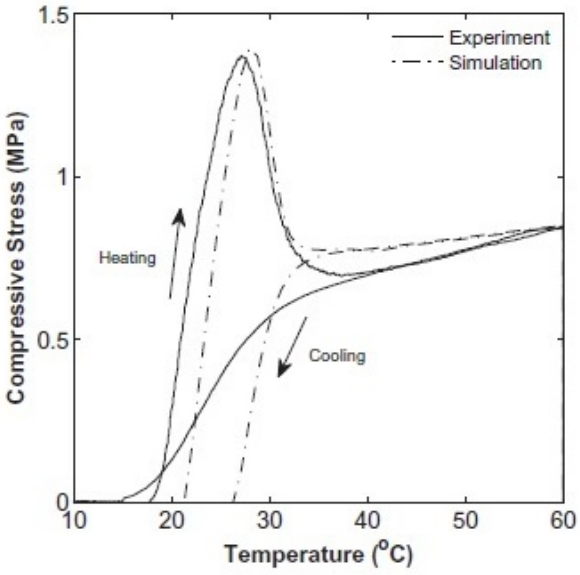


Figure 13: Stress response in the constrained recovery case [13].

## 5. Modeling in the frequency domain

The increasing use of SMP for dynamic applications, under various temperature ranges, has made necessary the characterization of these materials over wide frequency bands [17]. A dynamic mechanical analysis (DMA) can be used to determine the evolution of viscoelastic properties as a function of the temperature and loading frequency. The main purpose of this section is to check the validity of the time-temperature equivalence [18] obtained from the DMA measurements, use this equivalence to find the master curves of the material, and finally identify a suitable model for the viscoelastic behavior of the SMP.

### *5.1. Material and mechanical tests*

As a representative thermally-actuated shape-memory polymer, the tBA-/PEGDMA is chosen, it is a chemically-crosslinked thermoset polymer studied recently by Yakacki et al. [19] and Srivastava et al. [20].
This SMP is tested by a dynamic mechanical analysis. Viscoelastic properties (storage modulus $E'$, loss modulus $E''$ and loss factor $\tan(\delta)$) are measured using a METRAVIB DMA50 apparatus every 5 ℃ or 10 ℃ in isothermal conditions. Temperature varies between 0 ℃ and 90 ℃ and the frequency of

the excitation from 0.1 Hz to 180 Hz according to the temperature.
The results of the DMA tests are shown in figure 14. The storage modulus $E'$ decreases with the temperature and increases with the frequency. The large gap between the glass state modulus and the rubbery modulus (the ratio exceeds 3000), is a specificity of shape memory polymers. The glass transition temperature $T_g$ is located between 45 ℃ and 55 ℃. In this range of temperature, the viscoelastic properties of the tBA/PEGDMA are really interesting, indeed the value of the loss factor is higher than 1.5 in a wide range of frequencies and can reach a maximal value of 2.5 [21], which is much higher than classical materials used for vibration damping applications.

*5.2. Master curve*

According to the time-temperature superposition principle, curves of $E'$ and $\tan(\delta)$ vs. frequency (figure 14) at one temperature can be shifted horizontally to overlap with adjacent curves. The shift factors $a_T$ are obtained through an optimization procedure (classical least square method) for a reference temperature $T_0$ selected arbitrarily and are equivalent for both $E'$ and $\tan(\delta)$, therefore the time-temperature equivalence is validated in the considered temperature and frequency ranges for the tBA/PEGDMA. The master curves of the storage modulus and loss factor are given in figure 15.

In this work,the temperature evolution of the shift factor $a_T$ is expressed according to WLF equation (39) which can also be written as

$$\frac{T - T_0}{\log a_T} = -\frac{1}{C_1^0}(T - T_0) - \frac{C_2^0}{C_1^0}, \tag{42}$$

with $C_1^0 = 10.87$ and $C_2^0 = 32.57$ K for a reference temperature $T_0$ of 40 ℃ (figure 16).

*5.3. Modeling of viscoelastic behavior*

Two models are proposed here: the fractional derivative Zener model and the 2S2P1D. The Zener model [22] provides the expression of the elastic complex modulus as

$$E^*(\omega) = \frac{E_0 + E_\infty (i\omega\tau)^\alpha}{1 + (i\omega\tau)^\alpha}. \tag{43}$$

Its behavior in the frequency domain is described between two asymptotic values, namely the static elastic modulus $E_0$ and the high-frequency limit value of the dynamic modulus $E_\infty$ ; $\tau$ is the relaxation time and $\alpha$ is the order

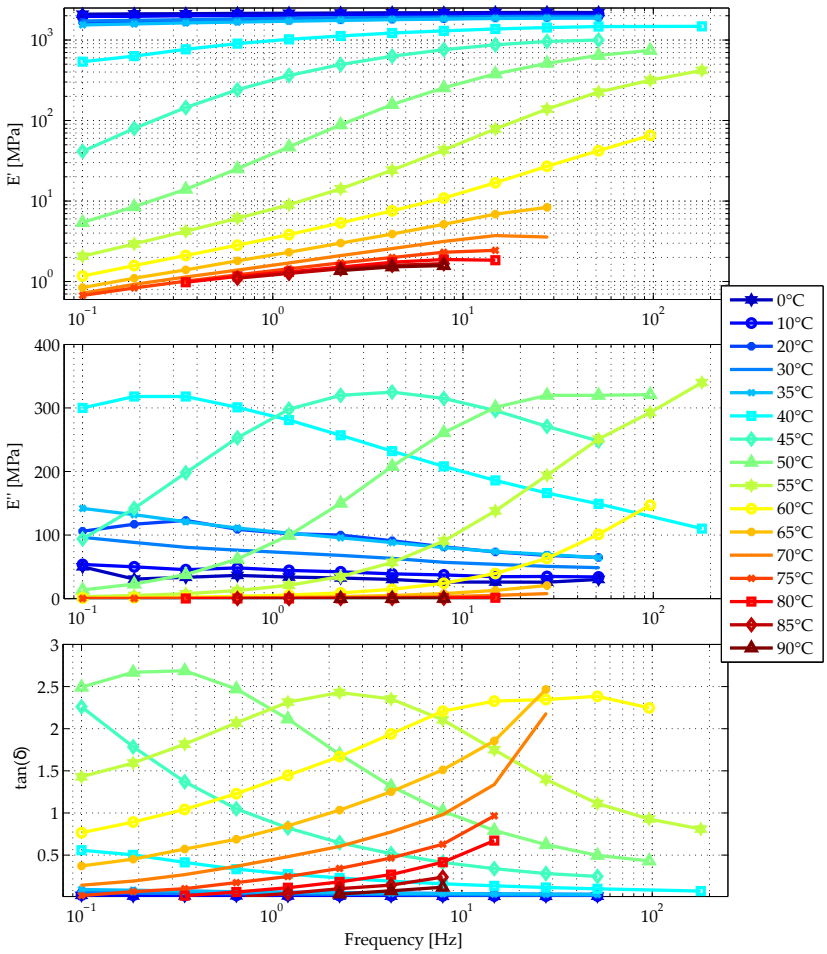


Figure 14: Storage modulus $E'$, loss modulus $E''$ and loss factor $\tan(\delta)$ measured by DMA according to the frequency $f$ and for several temperatures.

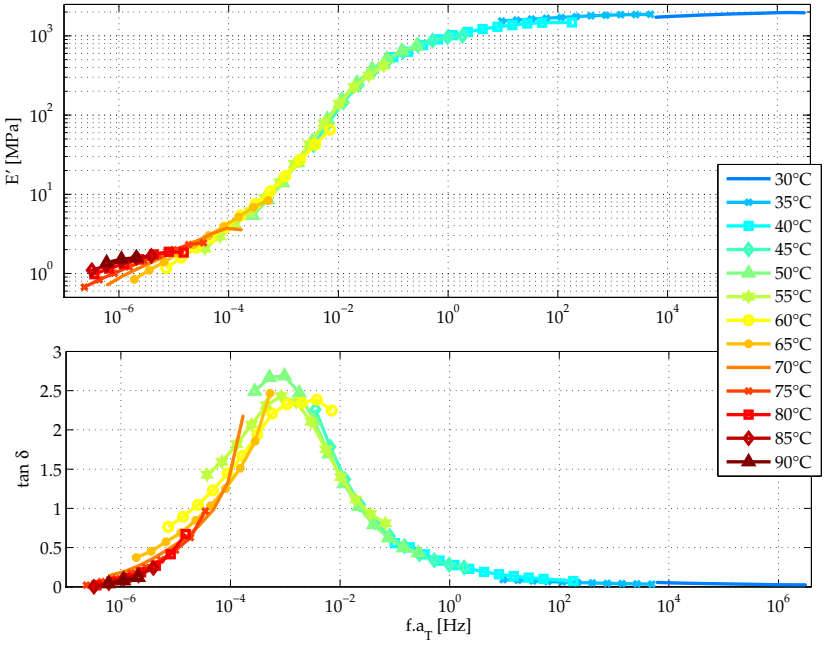


Figure 15: Master curves of $E'$ and $\tan(\delta)$ according to the reduced frequency $f.a_T$ with a reference temperature of 40 ℃.

of the fractional derivative. The statements $0 < \alpha < 1$, $\tau > 0$ and $E_\infty > E_0$ must hold to fulfill the second law of thermodynamics. An estimation of the four parameters $E_0$, $E_\infty$, $\alpha$ and $\tau$ from experimental measurements is given in [23]. The parameters of the fractional derivative Zener model obtained for the tBA/PEGDMA are given in Tab. 2, with $\tau(T) = a_T(T).\tau_0$.

The figure 17 compares the master curves of the dynamical properties (storage modulus, loss modulus and loss factor) obtained from experimental measurements with the ones coming from the Zener model, given by Equation 43). The viscoelastic behavior of the tBA/PEGDMA, predicted by the Zener model with only four parameters, seems reliable for the storage modulus and the loss factor. Moreover, the identification of the 4 parameters is obvious. However, the loss modulus and a close look at the transition region indicates that the Zener model is not able to represent the asymmetry of the $\tan(\delta)$ peak. This is the reason why a more general model, the 2S2P1D, is proposed. The 2S2P1D model, whose name comes the abbreviation of the combination of two springs, two parabolic creep element and one dashpot [24], is a model

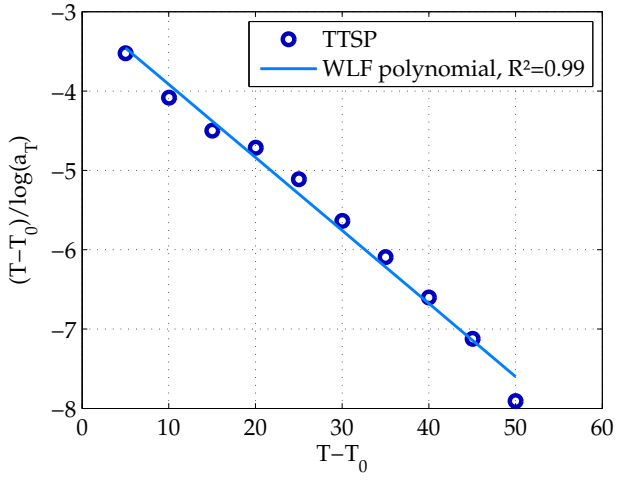


Figure 16: $a_T$: experimental data from dynamic analysis and WLF equation

Table 2: Zener model parameters for the SMP tBA/PEGDMA.

| $E_0$ (MPa) | $E_\infty$ (MPa) | $\alpha$ | $\tau_0$ (s) |
|---|---|---|---|
| 1 | 2200 | 0.78 | 1.22 |

allowing description of the rheological properties of a viscoelastic material with an asymmetric loss factor. For a given temperature, the 2S2P1D model is based on seven parameters, all with a physical meanings, to estimate the value of the complex modulus as

$$E^*(i\omega\tau) = E_0 + \frac{E_\infty - E_0}{1 + \gamma(i\omega\tau)^{-k} + (i\omega\tau)^{-h} + (i\omega\beta\tau)^{-1}}, \tag{44}$$

where $k$ and $h$ are exponents with $0 < k < h < 1$, $\gamma$ and $\beta$ are constants, $E_0$ is the rubber modulus when $\omega \to 0$, $E_\infty$ is the glassy modulus when $\omega \to \infty$ and $\tau$ is the characteristic time. The parameters are estimated using an optimization procedure based on least squares, directly from experimental data. For the tBA/PEGDMA the parameters are given in Table 3.

As can be seen from figure 17, a good fit is obtained between the 2S2P1D and the experimental measurements, on a wide frequency band. Compared

Table 3: 2S2P1D model parameters for the SMP tBA/PEGDMA

| $E_0$ (MPa) | $E_\infty$ (MPa) | $k$ | $h$ | $\gamma$ | $\beta$ | $\tau_0$ (s) |
|---|---|---|---|---|---|---|
| 1.01 | 2190 | 0.17 | 0.79 | 1.43 | 3.1e+4 | 0.83 |

to the Zener model, this model requires more efforts for parameters identification, but the result is really consistent with the experimental tests.

Among the various possible applications of using SMP for damping applications, a composite structure with tunable damping has been proposed in [21].

## 6. Conclusion

In this paper, several thermodynamical models have been reviewed from the literature, allowing description of time behavior of shape memory polymers in the time domain. A model suitable for frequency domain analyses has also been described, after some investigation that could show that time-temperature superposition principle was valid for the shape memory polymer of interest.

## Acknowledgements

The work of Pauline Butaud was co-financed by The French National Research Agency under Grant No. ANR-12-JS09-008-COVIA. It has been performed in cooperation with the Labex ACTION program (ANR-11-LABX-0001-01).

## Bibliography

[1] C. Lexcellent. *Shape-memory Alloys Handbook*. Wiley- ISTE, 2013.

[2] P. Butaud. *Contribution l'utilisation des polymères à mémoire de forme pour les structures à amortissement contrôlé.* PhD thesis, Université de Franche-Comté, 2015.

[3] S. Hayashi. Properties and applications of polyeuretane-series shape memory polymers. *Int. Prog.Urethanes*, 6:90–115, 1993.

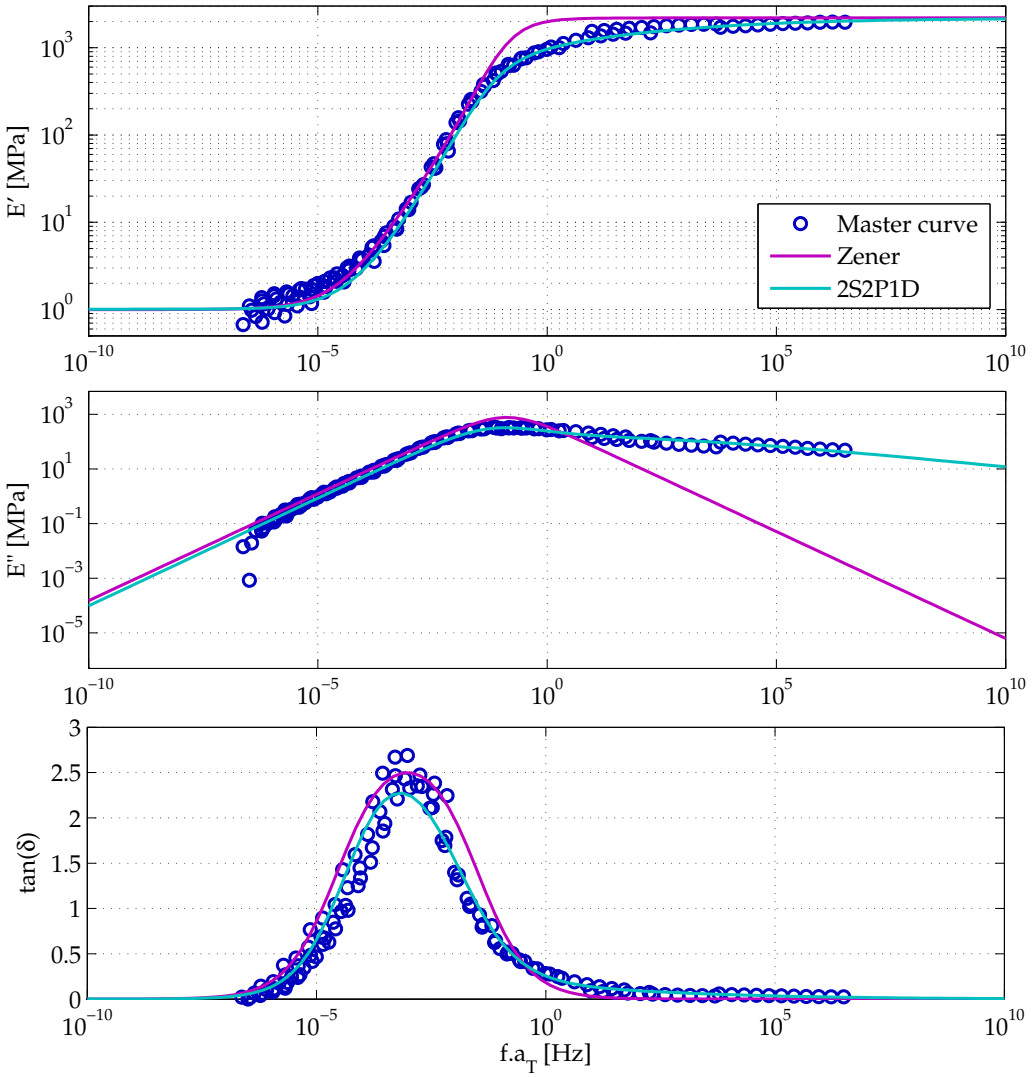


Figure 17: Master curves of tBA/PEGDMA for $T_0$ =40 ℃ compared with the Zener model ant the 2S2P1D model.

[4] E. A. Pieczyska, M. Staszczak, K. Maj, M.and Kowalczyk-Gajewska, K. Golasinki, M. Cristea, H. Tobushi, and S. Hayashi. Investigation of thermomechanical couplings, strain localization and shape memory polymer subjected to loading at various strain rates. *Smart Mater. Struct.*, 25, 2016.

[5] H. Tobushi, K. Okumora, S. Hayashi, and N. Ito. Thermomechanical model of shape memory polymer. *Mech. of Mat.*, 33:545–554, 2001.

[6] H. Qi, T.D Nguyen, C.M. Castro, F. Yakacki, and Shandas R. Finite deformation thermo-mechanical behavior of thermally induced shape memory polymers. *Journal of the Mechanics and Physics of Solids*, 56:1730–1751, 2008.

[7] E.M. Arruda and M.C. Boyce. A three-dimensional constitutive model for the large strecht behavior of elastomers. *J .Mech. Phys. Solids*, 41:650–664, 1993.

[8] A. Cohen. A pad approximant to the inverse langevin function. *Rheologica Acta*, 30(3):270–273, 1991.

[9] R. Jedynak. Approximation of the inverse langevin function revisited. *Rheologica Acta*, 54(1):29–39, 2015.

[10] Y.P Liu, M.L. . Gall, K.and Dunn, A.R. Greenberg, and J. Diani. Thermomechanics of shape memory plymers : uniaxial experiments and constitutive modeling. *Int. J.of Plasticity*, 22(2):279–313, 2006.

[11] E. A. Pieczyska, K. Maj, M.and Kowalczyk-Gajewska, M. Staszczak, A. Gradys, M. Majewski, H. Cristea, M. Tobushi, and S. . Hayashi. Thermomechanical properties of polyurethane shape memory polymer-experiment and modeling. *Smart Mater. Struct.*, 24, 2015.

[12] P. Gilormini and J. Diani. On modeling shape memory polymers as thermoelastic two-phse composite materials. *Compte Rendu de l'Acadmie des Sciences : Mcanique*, 340:338–348, 2012.

[13] K. Westbrook, P.H. Kao, F. Castro, Y. Ding, and J.H. Qi. A 3d finite constitutive model for amourphous shape memory polymers : A multi-branch modeling for nonequilibrium relaxation processes. *Mech. of Mat.*, 43:853–869, 2011.

[14] M. Rubinstein and R.H. Colby. *Polymer Physics*. Oxford University Press, Oxford ; New York, 2003.

[15] M.L. Williams, R.F. Landel, and J.D. Ferry. Temperature dependence of relaxation mechanisms in amorphous polymers and other glass-classic forming liquids. *Physical Review*, 98:1549, 1955.

[16] E.A. Di Marzio and A.J.M. Yang. Configurational entropy appraach to the kinetics of glasses. *Journal of Research of the National Institute of Standards and Technology.*, 102:135–157, 1997.

[17] P Butaud, V Placet, J Klesa, M Ouisse, E Foltête, and X Gabrion. Investigations on the frequency and temperature effects on mechanical properties of a shape memory polymer (veriflex). *Mechanics of Materials*, 87:50–60, 2015.

[18] N. Okubo. Preparation of Master Curves by Dynamic Viscoelastic Measurements. *SII NanoTechnology Inc.*, 6, 1990.

[19] Christopher Michael Yakacki, Robin Shandas, Craig Lanning, Bryan Rech, Alex Eckstein, and Ken Gall. Unconstrained recovery characterization of shape-memory polymer networks for cardiovascular applications. *Biomaterials*, 28(14):2255 – 2263, 2007.

[20] Vikas Srivastava, Shawn a. Chester, and Lallit Anand. Thermally actuated shape-memory polymers: Experiments, theory, and numerical simulations. *Journal of the Mechanics and Physics of Solids*, 58(8):1100–1124, August 2010.

[21] Pauline Butaud, Emmanuel Foltête, and Morvan Ouisse. Sandwich structures with tunable damping properties: On the use of shape memory polymer as viscoelastic core. *Composite Structures*, 153:401–408, 2016.

[22] L Rouleau, J-F Deü, A Legay, and J-F Sigrist. Vibro-acoustic study of a viscoelastic sandwich ring immersed in water. *Journal of Sound and Vibration*, 331(3):522–539, 2012.

[23] AC Galucio, J-F Deü, and R Ohayon. Finite element formulation of viscoelastic sandwich beams using fractional derivative operators. *Computational Mechanics*, 33(4):282–291, 2004.

[24] Nur Izzi Md. Yusoff, Damien Mounier, Ginoux Marc-Stphane, Mohd. Rosli Hainin, Gordon D. Airey, and Herv Di Benedetto. Modelling the rheological properties of bituminous binders using the 2s2p1d model. *Construction and Building Materials*, 38(0):395 – 406, 2013.